Supporting Information

Encapsulating Si nanoparticles in ZIF-8-derived carbon through surface amination for stable lithium storage

Le Li [a, b], Jinshuai Liu [a, b], Ruohan Yu [a, b], Ruhan He [a], Jinghui Chen [a, b], Haoqing Ma [a, b], Lei Zhang [a, b], Liqiang Mai [a, b, *], Liang Zhou [a, b, *]

[a] The Sanya Science and Education Innovation Park, Wuhan University of Technology, Sanya 572000, China

[b] State Key Laboratory of Advanced Technology for Materials Synthesis and Processing, Wuhan University of Technology, Wuhan 430070, China

Experimental Section

Synthesis of NH_2-Si.

Typically, 0.2 g of Si nanoparticles were dispersed in 200 mL of deionized water under ultrasonication for 1h. After ultrasonication, 0.8 mL of (3-aminopropyl)trimethoxysilane (APTMS) was added to the solution. Then the mixture was intensely stirred for 18 h at room temperature. After that, the precipitate was collected by centrifugation and washed with ethanol three times. Subsequently, the solid was redispersed in 300 mL of aqueous polyvinyl pyrrolidone (PVP) solution (0.2 wt%). Finally, the precipitate was centrifuged three times at 8000 rpm and dried at 80 °C under vacuum for 12 h.

Synthesis of NH_2-Si@ZIF and Si@ZIF.

To synthesize the NH_2-Si@ZIF precursor, 2.97 g of $Zn(NO_3)_2 \cdot 6H_2O$ and 200 mg of NH_2-Si were dissolved in 75 mL of methanol as solution A. Solution B was prepared by dissolving 3.284 g of 2-MI in 25 mL methanol. Solution A and B were mixed under constant stirring at room temperature for 24 h. Then, the NH_2-Si@ZIF powder was collected by centrifugation and washed with ethanol three times. Subsequently, the solid was dried at 80 °C under vacuum for 12 h to obtain NH_2-Si@ZIF. The Si@ZIF was synthesized by replacing NH_2-Si with pure Si nanoparticles under the same conditions.

Synthesis of NH_2-Si@C and Si@C.

The collected precursor (NH_2-Si@ZIF and Si@ZIF) was annealed at 900 °C for 2 h in N_2 to obtain NH_2-Si@C and Si@C.

Materials characterizations

Scanning electron microscopy (SEM) images were collected on a JEOL-7100F field emission scanning electron microscope, while transmission electron microscopy (TEM), high-resolution TEM (HRTEM), and high-angle annular dark-field scanning TEM (HAADF-STEM) images were obtained on JEM-2100F and Titan Themis3 G2 300. X-ray diffraction (XRD) analysis was carried out on a Bruker D8 Discover X-ray diffractometer with a Cu Kα X-ray source (λ = 1.5418 Å). Raman spectra were recorded on a Renishaw INVIA Raman microscope with a 532-nm laser. Thermogravimetric analysis (TGA) was acquired via an STA-449C thermobalance with a heating rate of 5 °C min^{-1} in air. X-ray photoelectron spectroscopy (XPS) characterizations were performed on a VG Multilab 2000 with an Al Kα monochromated X-ray source. Fourier-transform infrared (FT-IR) spectra were obtained on a Nicolet 6700 IR spectrometer.

Electrochemical measurement

The working electrodes consisted of active materials (70 wt%),

acetylene black (15 wt%), and polyacrylic acid (15 wt%) coated on Cu foil. The coin-type half-cells (CR2016) were assembled in an Ar-filled glove box. $LiPF_6$ (1.0 mol L^{-1}) in ethylene carbonate/ diethyl carbonate/ dimethyl carbonate (1:1:1 in volume) with 10 vol% fluoroethylene carbonate (FEC) was used as the electrolyte. Galvanostatic charge-discharge (GCD) measurements (0.01–1.5 V vs. Li^+/Li) were performed on a LAND CT2001A multichannel battery testing system. Cyclic voltammetry (CV) profiles were obtained on an Autolab Potentiostat Galvanostat (PGSTAT 302N) workstation at a scan rate of 0.1 mV s^{-1}. Electrochemical impedance spectroscopy (EIS) curves were collected with a frequency range of 0.01 Hz to 100 kHz with a potential amplitude of 10 mV.

In-situ characterizations

The electrodes for the *in-situ* XRD study were composed of active materials (60 wt%), acetylene black (30 wt%), and polytetrafluoroethylene (PTFE, 10 wt%). *In-situ* XRD experiments were performed on a D8 Discover X-ray diffractometer equipped with a planar detector. The anode was placed on the back side of an X-ray transparent Be window which also served as the current collector. The *in-situ* XRD signals were collected in the range of 25°–60° with a still mode. Each pattern was acquired in 120 s.

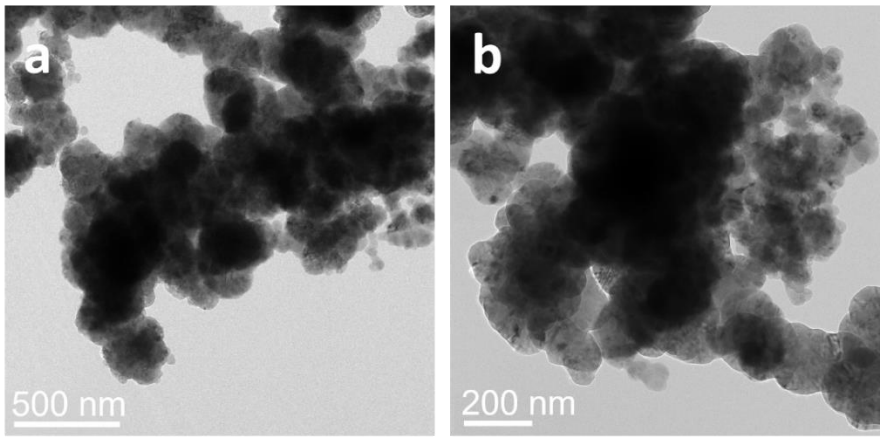

Fig. S1. TEM images of pure Si.

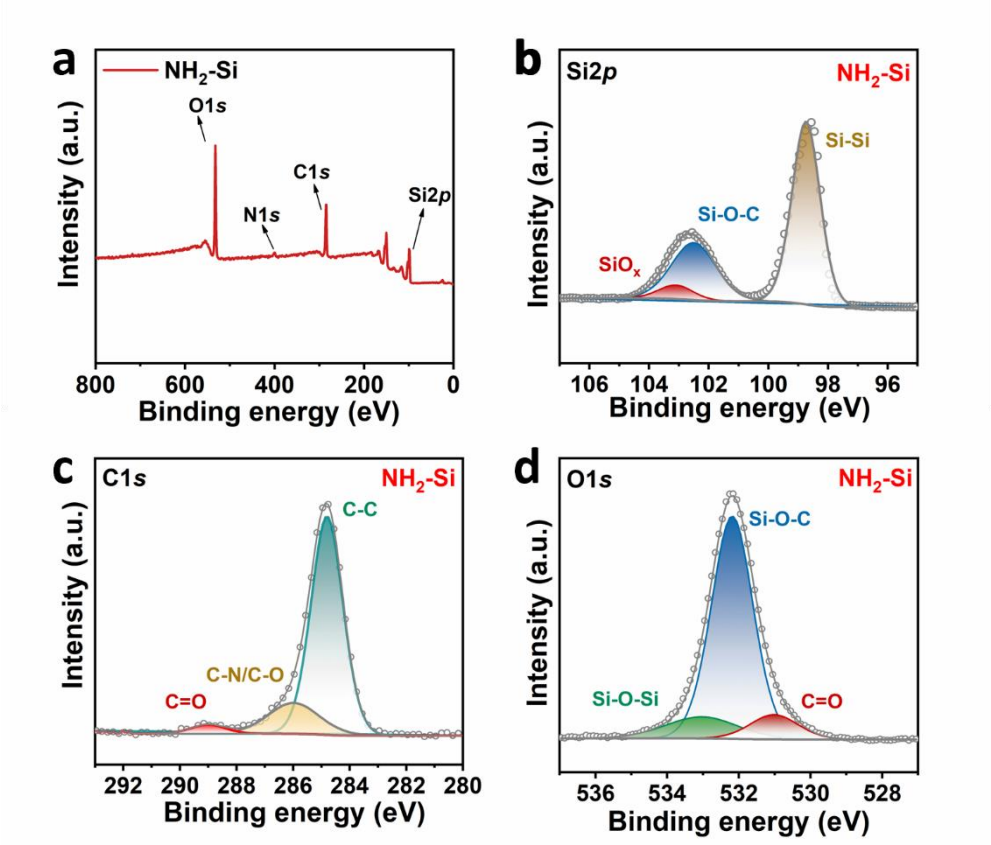

Fig. S2. (a) XPS survey spectra of NH_2-Si; (b) Si 2p (c) C 1s and (d) O 1s XPS spectra of NH_2-Si.

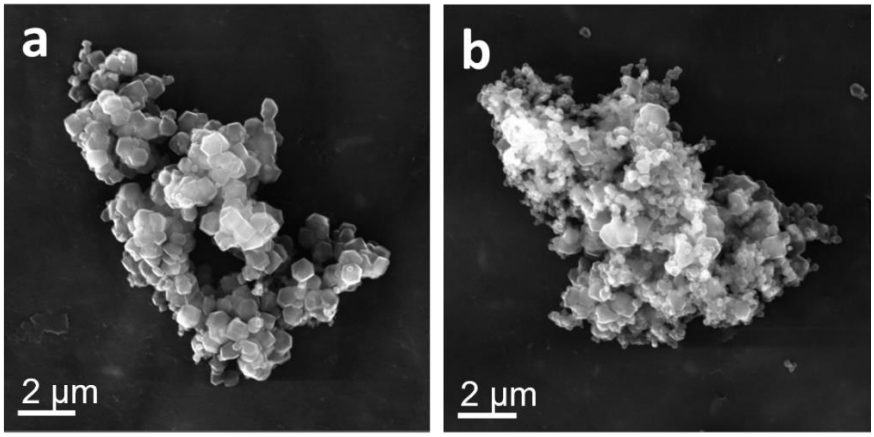

Fig. S3. SEM images of (a) Si-ZIF and (b) Si@C.

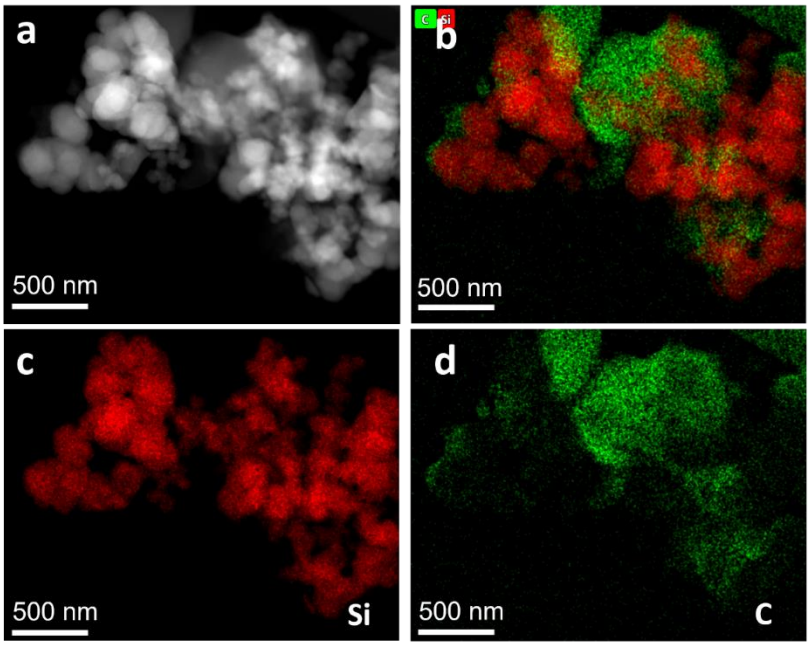

Fig. S4. (a) HAADF-STEM image, and (b–d) EDS mappings (corresponding to a) of Si@C.

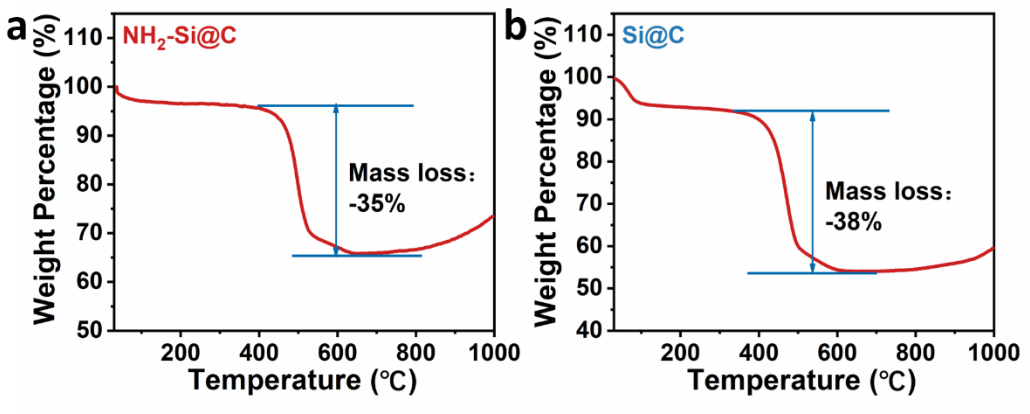

Fig. S5. TGA curves of (a) NH_2-Si@C and (b) Si@C.

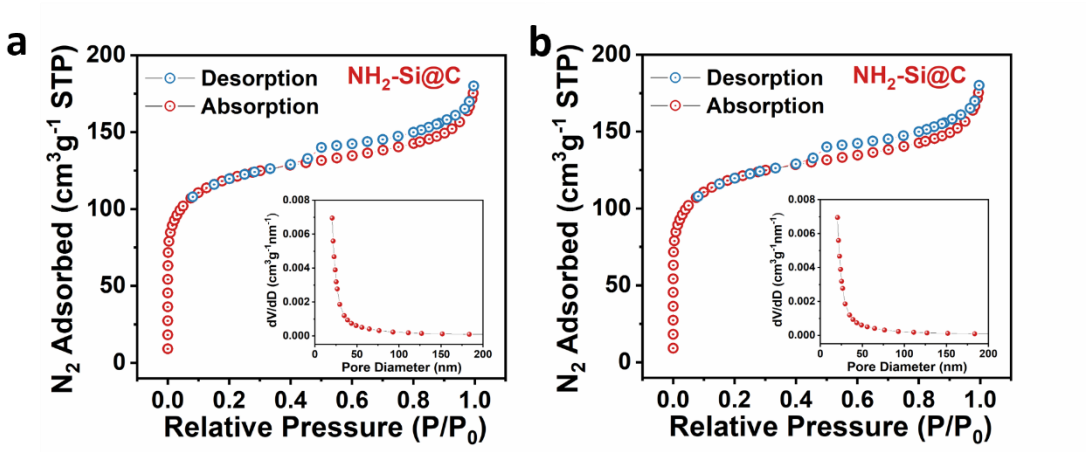

Fig. S6. N_2 adsorption/desorption isotherms and pore-size distribution curves (inset in (a, b)) of (a) NH_2-Si@C and (b) Si@C.

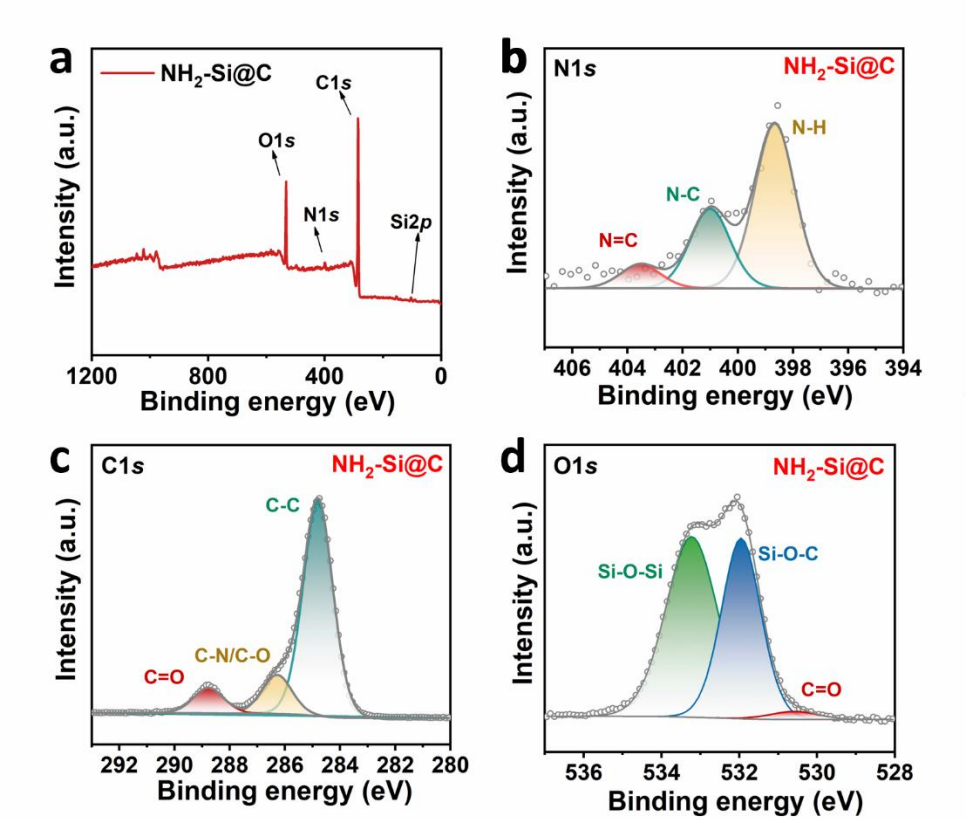

Fig. S7. (a) XPS survey spectra of NH_2-Si@C; (b) N 1s, (c) C 1s, and (d) O 1s XPS spectra of NH_2-Si@C.

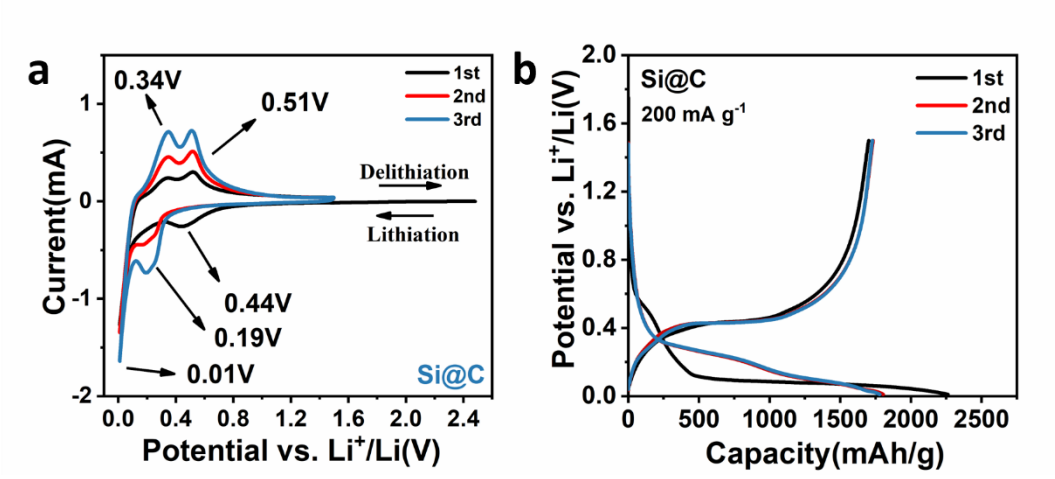

Fig. S8. (a) CV profiles and (b) representative GCD profiles of Si@C.

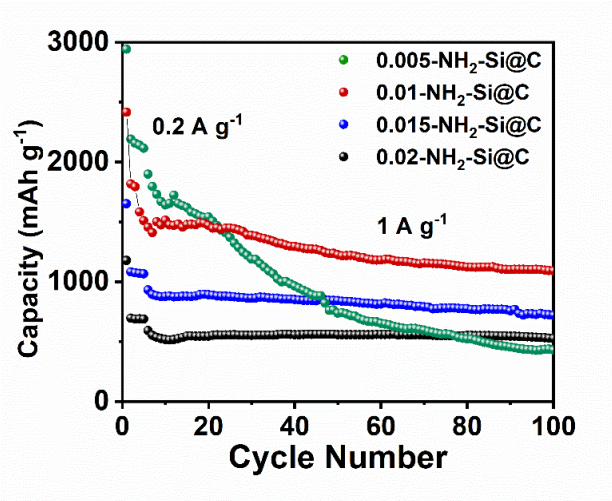

Fig. S9. The electrochemical performance of the NH_2-Si@C composites with different content of ZIF-8.

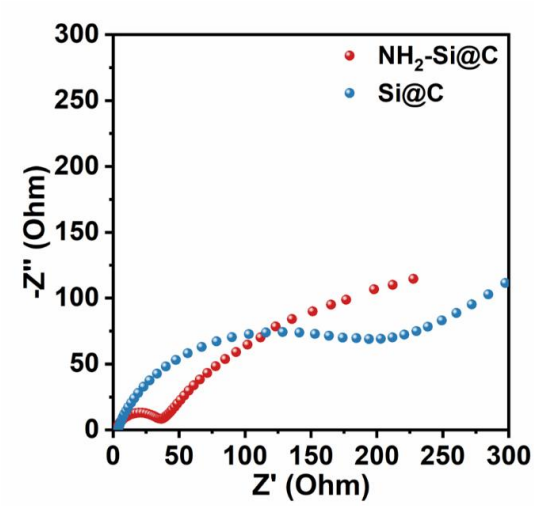

Fig. S10. The electrochemical impedance spectroscopy plots of NH_2-Si@C and Si@C. The Nyquist plots were collected in a frequency range of 0.01 Hz to 10 kHz.

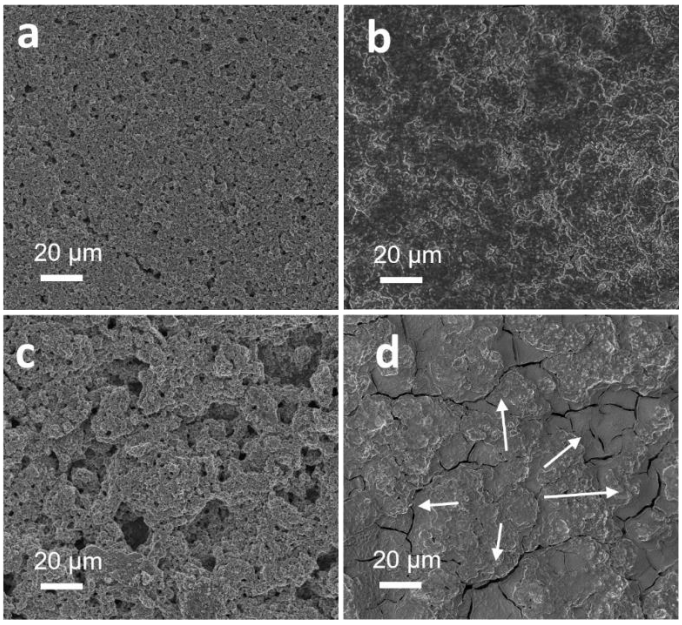

Fig. S11. Top-view SEM images of NH_2-Si@C (a) before and (b) after 50 cycles at 1 A g^{-1}, top-view SEM images of Si@C (c) before and (d) after 50 cycles at 1 A g^{-1}.

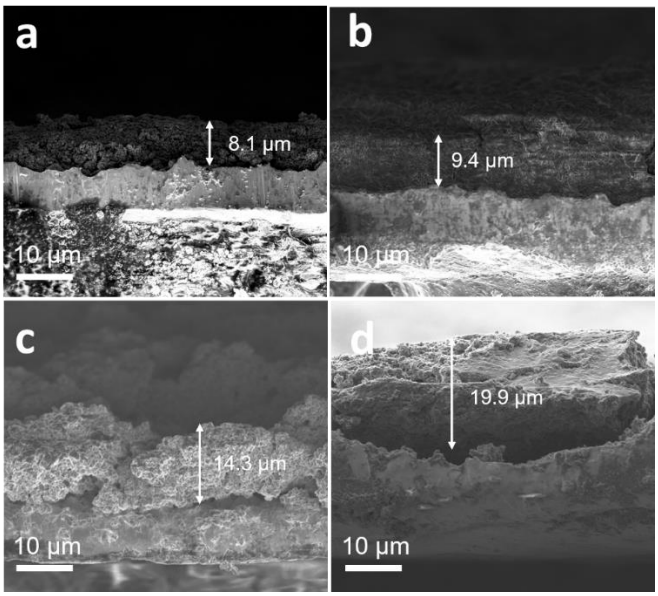

Fig. S12. Cross-sectional SEM images of NH_2-Si@C-based electrode (a) before and (b) after 50 cycles at 1 A g^{-1}, cross-sectional SEM images of Si@C-based electrode (c) before and (d) after 50 cycles at 1 A g^{-1}.

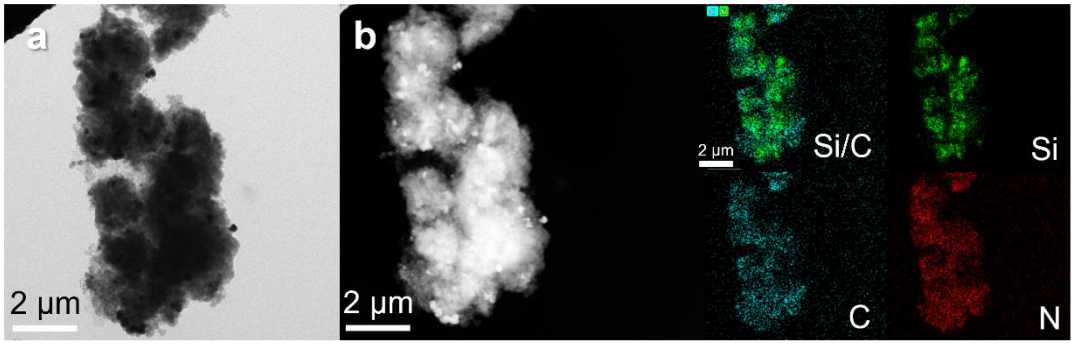

Fig. S13. (a) TEM image, (b) HAADF image, and the corresponding elemental maps of NH_2-Si@C after 100 cycles at 1 A g^{-1}.

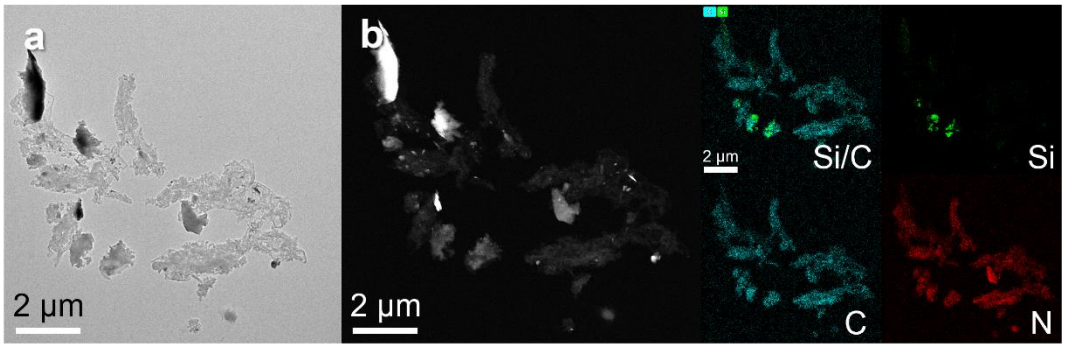

Fig. S14. (a) TEM image, (b) HAADF image, and the corresponding elemental maps of Si@C after 100 cycles at 1 A g^{-1}.

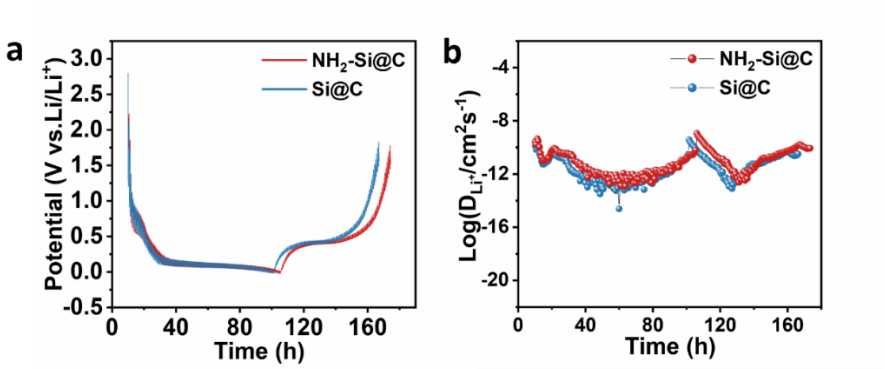

Fig. S15. (a) GITT curves of NH_2-Si@C and Si@C; (b) lithium-ion diffusion coefficients of NH_2-Si@C and Si@C.

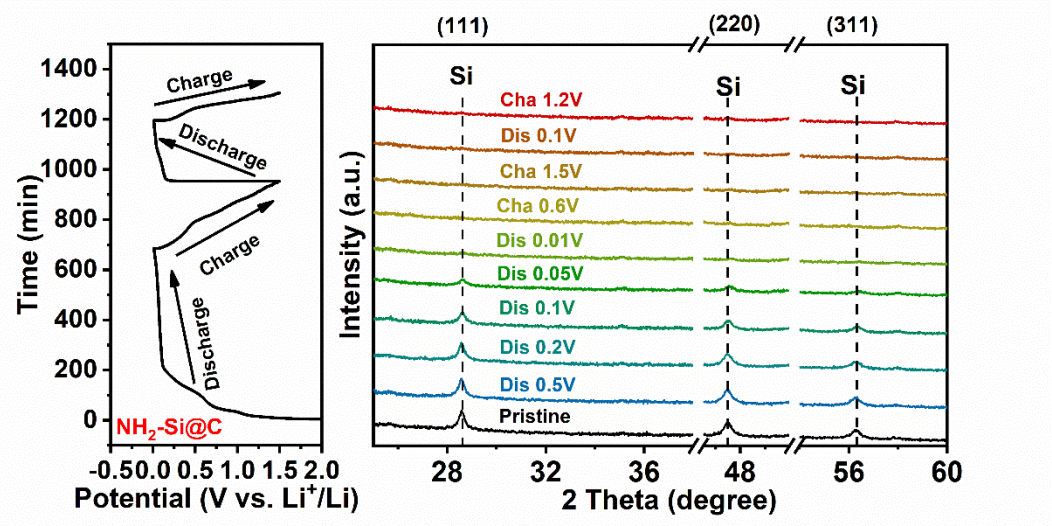

Fig. S16. *In-situ* XRD patterns of NH_2-Si@C during the first two discharging/charging cycles.

Table S1 Comparison of the electrochemical performances of NH_2-Si@C with previously reported Si/ZIF derived composite anodes.

Materials	Si Content (wt.%)	Cycling ($mAh\ g^{-1}$)	Rate ($mAh\ g^{-1}$)	ICE (%)
This work	**65**	**991 after 300 cycles at 1.0 A g^{-1}**	**1062 at 5 A g^{-1}**	**75.8**
Si@ZIF-8-700N [1]	–	830 after 500 cycles at 0.2 A g^{-1}	300 at 3.2 A g^{-1}	–
H-Si@C [2]	81.1	1009 after 200 cycles at 1 A g^{-1}	678 at 5 A g^{-1}	78.5
Si@NC [3]	6.6	302 after 800 cycles at 1 A g^{-1}	139 at 5 A g^{-1}	54.4
3D Si/NGC [4]	38	900 after 300 cycles at 0.2 A g^{-1}	880 at 1 A g^{-1}	56
Si@$CoSi_2$/Co-	37.67	57.3% after 500	930 at 6 A g^{-1}	76.1

NPC@CNT [5]		cycles at 1 A g^{-1}		
Si@c-ZIF@CNFs [6]	31.4	518.6 after 1000 cycles at 1 A g^{-1}	523.9 at 5 A g^{-1}	77
Si@8Z [7]	91.3	818.5 after 650 cycles at 1 A g^{-1}	824.3 at 8 A g^{-1}	88.2

References

[1] Y. Han, P. Qi, X. Feng, S. Li, X. Fu, H. Li, Y. Chen, J. Zhou, X. Li, B. Wang, ACS Appl. Mater. Interfaces 7 (2015) 2178–2182.

[2] H. Xue, Y. Wu, Z. Wang, Y. Shen, Q. Sun, G. Liu, D. Yin, L. Wang, Q. Li, J. Ming, ACS Appl. Mater. Interfaces 13 (2021) 40471–40480.

[3] Q. Li, Y. Wang, X. Gao, H. Li, Q. Tan, Z. Zhong, F. Su, J. Alloys Compd. 872 (2021) 159712.

[4] T. Mu, P. Zuo, S. Lou, Q. Pan, H. Zhang, C. Du, Y. Gao, X. Cheng, Y. Ma, H. Huo, G. Yin, J. Alloys Compd. 777 (2019) 190–197.

[5] Y. Qiu, C. Zhang, C. Zhang, Q. Xie, Z. Qiao, X. Zeng, W. Xu, H. Zheng, S. Li, J. Lin, D.L. Peng, J. Alloys Compd. 877 (2021) 160240.

[6] J. Chen, X. Guo, M. Gao, J. Wang, S. Sun, K. Xue, S. Zhang, Y. Liu, J. Zhang, Chem. Commun. 57 (2021) 10580–10583.

[7] D. Zhang, R. Yang, J. Zhou, W. Liu, H. Qin, Z. Zhang, X. Lei, A. Lu, Z. Mo, L. Miao, F. Dang, Energy Storage Mater. 63 (2023) 102976.